MATERIALS SCIENCE

Programmable wettability on photocontrolled graphene film

Jie Wang[1], Wei Gao[2], Han Zhang[1], Minhan Zou[1], Yongping Chen[3,2]*, Yuanjin Zhao[1]*

Surface materials with specific wettability play important roles in a wide variety of areas from science to industry. We present a novel paraffin-infused porous graphene film (PIPGF) with programmable wettability. Because of graphene's photothermal property, the paraffin in the PIPGF was in transition between liquid and solid in response to near-infrared (NIR) light irradiation. Thus, we imparted the film with a dynamic and reversible transition between a slippery and a rough surface as the remotely tunable wettability. In addition, with the integration of NIR masks, the paraffin could melt at corresponding patterns on the PIPGF, which formed special flow pathways for the slipping droplets. Therefore, the PIPGF could provide programmable wettability pathways for the spatiotemporal droplet manipulation by flexibly changing the NIR masks. We demonstrated these programmable wettability pathways to not only simplify liquid handling in the microplates and droplet microarrays technology but also to provide distinctly microfluidic microreactors for different purposes, such as practical blood grouping diagnosis. These features indicated that the photocontrollable PIPGF would be amenable to a variety of applications, such as microfluidic systems, laboratory-on-a-chip settings, and droplet manipulations.

INTRODUCTION

Surfaces with specific wettability have attracted remarkable attention in recent years for their broad technological implications in the areas of energy, environment, and health (*1*–*9*). Inspired by natural organisms, various functional surfaces with special wettability properties have been developed by mimicking these natural constructions (*10*–*15*). Among these, slippery liquid-infused porous surfaces (SLIPSs) could be considered one of the most prominent examples that outperformed their natural counterparts and provided state-of-the-art surfaces with stable and defect-free repellency for various simple and complex liquids (*16*–*20*). In particular, SLIPSs with tunable wettability that can dynamically manipulate the mobility of liquid droplets on surfaces have been achieved by infusing adaptive liquids into porous elastomer films to further broaden their applications (*21*–*24*). Although with many improvements and the contact-based control methods have been discovered in existing tunable slippery surfaces, their noncontact regulation that can provide spatial and temporal control is unrealized. In addition, a programmable slippery surface with flexible droplet sliding paths, which would be of revolutionary significance for microfluidic technology, is difficult to achieve based on the recent tunable wettability approaches. Thus, functional slippery surfaces with programmable wettability capable of manipulating droplets spatiotemporally are still being sought after.

Here, we present a novel paraffin-infused porous graphene film (PIPGF) with desired surface features. As an emerging carbon material, graphene and its derivatives have been investigated extensively for uses in different areas because of their extraordinary electrical, mechanical, optical, and thermal properties (*25*–*28*). Graphene-derived three-dimensional (3D) sponges also exhibited porous structures with high specific surface areas and extraordinary capacity for photothermal energy transformation (*29*–*32*). Thus, it is conceivable to infuse a porous graphene sponge with paraffin; this could achieve a reversible paraffin transition of solid and liquid with the photothermal effect of graphene under near-infrared (NIR) light irradiation (Fig. 1A). In this process, the droplets could slide down along the graphene film when the paraffin was heated to melting, but they were pinned on the film surface if the paraffin was cooled to solidification. Thus, the state of matter and the surface wettability of the PIPGF could be remotely controlled with high stability and fast reversibility by using NIR light. Attractively, with the integration of NIR masks, the paraffin could melt at corresponding patterns on the PIPGF, which formed special flow pathways for the slipping droplets (Fig. 1B). As the masks could be flexibly changed, the PIPGF could provide programmable wettability pathways for the spatiotemporally controllable droplet manipulation and reaction. It was demonstrated that these programmable wettability pathways could not only simplify liquid handling in the microplates and droplet microarrays technology but also provide distinct microfluidic microreactors for different purposes, such as practical blood grouping diagnosis. These features make the photocontrollable PIPGF versatile platforms for droplet manipulations in different areas.

RESULTS

In a typical experiment, we fabricated the 3D graphene [the main component was reduced graphene oxide (GO), which was referred to as "graphene" in this research] sponge film by constructing synergistic interface interactions of ionic bonding with Ca^{2+} during the gelation of a GO aqueous solution, which was reduced with the aid of hydroiodic acid (HI) and freeze-dried subsequently to form porous structures. We investigated the surface and cross section of the fabricated graphene sponge film by scanning electron microscopy (SEM) in Fig. 2 (A and B), which showed honeycomb-like architectures with high specific surface areas. The hydrophobic surface (Fig. 2E) and the porous network structure of graphene sponge film made it

[1]State Key Laboratory of Bioelectronics, School of Biological Science and Medical Engineering, Southeast University, Nanjing 210096, China. [2]Key Laboratory of Energy Thermal Conversion and Control of Ministry of Education, School of Energy and Environment, Southeast University, Nanjing 210096, China. [3]Jiangsu Key Laboratory of Micro and Nano Heat Fluid Flow Technology and Energy Application, School of Environmental Science and Engineering, Suzhou University of Science and Technology, Suzhou 215009, China.
*Corresponding author. Email: yjzhao@seu.edu.cn (Y.Z.); ypchen@mail.usts.edu.cn (Y.C.)

possible to infuse the melted paraffin liquid into the pores of the sponge to construct a slippery surface. Through capillary forces and matching chemistry between the paraffin liquid and solid graphene surface, the paraffin could uniformly cover the graphene scaffold, as shown in Fig. 2 (C and D). We found both the surface and the cross section of the graphene scaffold to be coated with paraffin, which showed apparent wrinkles. This result indicated the uniform coating of the paraffin on the graphene sponge film.

We found the graphene sponge film to have an extraordinary capacity for photothermal energy transformation under strong NIR optical absorption with a wavelength of 808 nm, and we generated a large amount of heat when the PIPGF was irradiated under NIR (fig. S1). Thus, the paraffin part that was exposed to NIR would become liquid when the ambient temperature was above the melting point of paraffin. However, as soon as the laser was switched off, the paraffin would cool down to the solid state again, showing little difference to before the NIR irradiation (compare fig. S1, D and F). These results indicated that the transition of paraffin from solid to liquid in the PIPGF could be remotely controlled with easy operation, high stability, and fast reversibility by using NIR light. It is worth mentioning that although other kinds of carbon materials, such as carbon nanotube and carbon black, have the NIR photothermal energy transformation property as well, their film formation is not as good as graphene, which restricts their application in this experiment.

To investigate the wettability of the fabricated PIPGF with the NIR switched on/off, we measured the contact and sliding angles of the water droplet on the PIPGF surface (Fig. 2, E to G). We found the water contact angle on the surface of the graphene sponge film to be 110° ± 1.4°, which demonstrated the hydrophobic surface property. After being infused with paraffin, the water contact angle on the PIPGF surface decreased to 79° ± 2.0° with NIR switched on and 102° ± 1.2° with NIR switched off. Besides the effect on the contact angle, the different condition of NIR also led to significant changes in the sliding angle of the droplets on the surface of the PIPGF (Fig. 2, F and G). With the laser switched on, the sliding angle of the water droplet was only 5°, which demonstrated good slippery properties. However, the sliding angle of the droplet trended toward 87° after the laser was turned off, and the ambient temperature was below the paraffin melting point. This was ascribed to the solidification of the paraffin, which changed the surface morphology of the PIPGF. Thus, we pinned the water droplets on the surface when the graphene film was tilted less than 87°. We further measured the sliding angles of the PIPGF during 20 cycles with the laser switched on/off, which demonstrated excellent cyclic reproducibility (Fig. 2H). Therefore, the PIPGF would present a reversible droplet pinning feature with NIR switched off and repellence for droplets with NIR switched on.

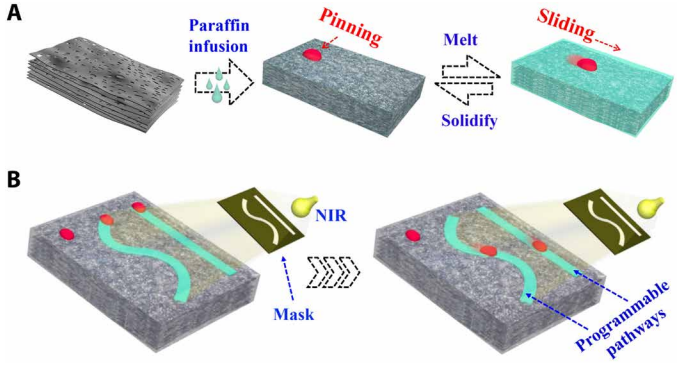

Fig. 1. Schematic diagram of the PIPGF with programmable wettability. (**A**) Tunable wettability of the PIPGF controlled remotely using NIR light. (**B**) Programmable wettability pathways on the surface of the PIPGF were formed with the integration of NIR masks for controllable droplet manipulation.

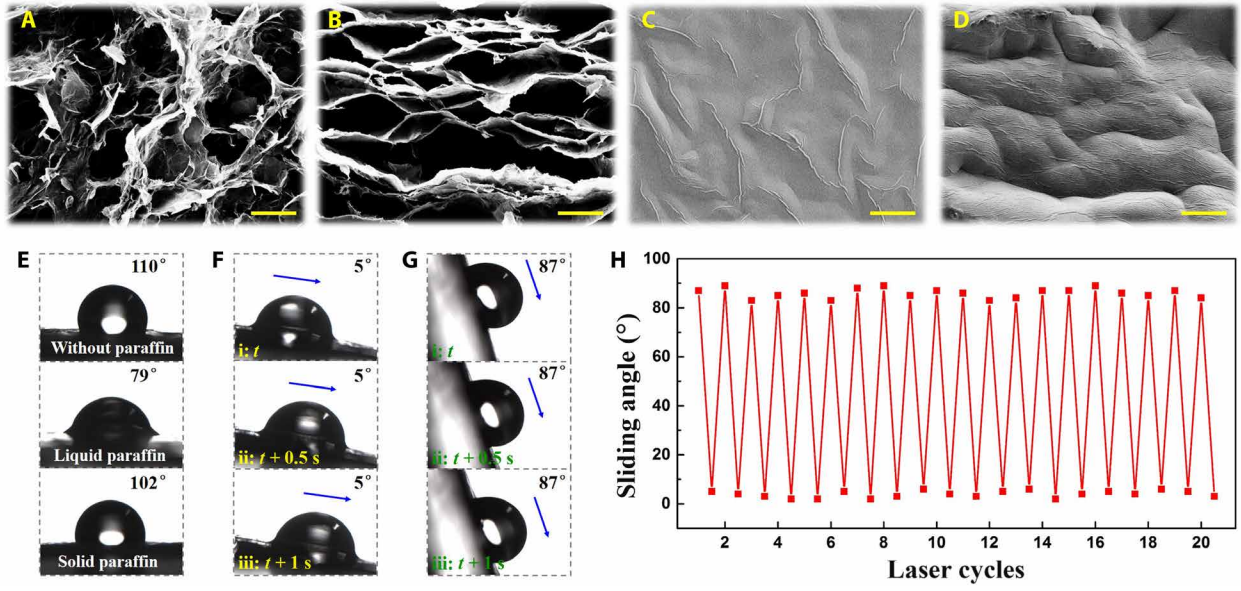

Fig. 2. Microstructures and wettability of the graphene sponge film and the PIPGF. (**A** to **D**) SEM images of (A and B) the graphene sponge film and (C and D) the PIPGF. (A) and (C) are the surfaces, and (B) and (D) are the cross sections of the corresponding film. (**E**) Measured water contact angles of the porous graphene sponge film, the PIPGF with laser switched on, and the PIPGF with laser switched off, respectively. (**F**) Progress of the water droplet sliding down the surface of the PIPGF with laser switched on; the sliding angle of which is 5°. (**G**) Progress of the water droplet sliding down the surface of the PIPGF with laser switched off; the sliding angle of which is 87°. (**H**) Water sliding angle variation of the PIPGF as a function of laser cycle numbers. Scale bars, 10 μm.

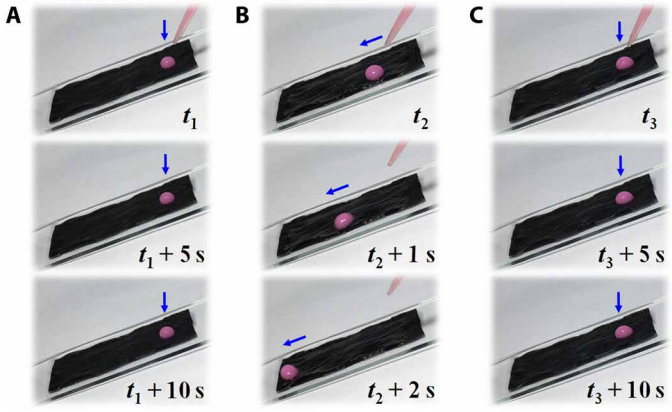

Fig. 3. Dynamic control of droplet mobility on a tilted PIPGF surface of 20°. (**A**) Progress of a water droplet pinned on the PIPGF at room temperature. (**B**) Progress of the water droplet sliding down the surface of the PIPGF with NIR switched on. (**C**) Progress of the droplet pinned on the PIPGF after NIR switched off.

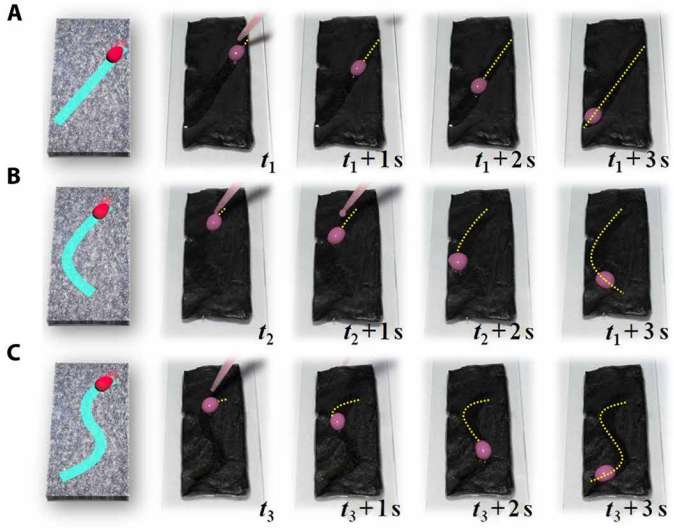

Fig. 4. Dynamic control of the droplet mobility on the PIPGF surface guided by designed pathways. (**A**) Oblique pathway, (**B**) arc pathway, and (**C**) S-shape pathway, respectively.

The NIR-controlled tunable wettability of the PIPGF provided a promising means to dynamically manipulate the mobility of droplets on the surface. As mentioned above, the dynamic paraffin-infused interface provided by the porous graphene film could reversibly transit between a slippery and a rough surface in response to NIR. To demonstrate this tunable function, we analyzed the dynamic wettability of the PIPGF by monitoring the liquid droplets on the surface, as recorded in Fig. 3 and movie S1. We observed that the droplet was pinned to the surface of the PIPGF at room temperature (Fig. 3A) but slid quickly down the substrate when exposed to NIR (Fig. 3B). However, we stopped the droplets and held them in place again on the surface when the laser was switched off (Fig. 3C). This novel PIPGF with on-demand tunable and reversible repellency paves the way for droplet manipulation technologies.

On the basis of their surface tunable wettability features, we further integrated the PIPGF with NIR masks to provide programmable wettability pathways for the spatiotemporal droplets manipulation on the surface, as shown in Fig. 4 and movie S2. The spatiotemporally control of liquid movement on a surface has attracted interest from science and industry because it plays significant roles in novel microfluidic systems for droplet harvesting, transportation, and manipulation technologies (*33*–*38*). To construct the liquid movement pathways, we here used NIR masks to block part of the laser light while allowing the other part to go through to the PIPGF surface. The NIR-irradiated paraffin part would melt at the corresponding patterns and become slippery, whereas the unirradiated part would remain rough. Thus, special surfaces with patterned wettability and designed flow pathways for the slipping droplets could be formed in correspondence with the NIR masks. Attractively, various kinds of droplet-guiding pathways could be designed depending on the different NIR mask styles, as shown in Fig. 4 (A to C). From the results, it could be found that the droplet-guiding pathways could change flexibly on the same PIPGF surface, which was of revolutionary significance for programmable spatiotemporal manipulating of droplets on the surface. It is worth mentioning that the surface temperature of the PIPGF could be monitored with the assistance of an infrared camera (figs. S2 and S3). This made it possible to find the optimal NIR irradiation conditions such as the irradiation intensity and distance that could solve the problem of overheating the PIPGF and effectively reduce the temperature restriction in practical applications. We also investigated the thickness of PIPGF, the GO concentration, the paraffin volume, and the volume ratio of paraffin to liquid paraffin, which might influence the melting and solidification times, in fig. S4. The results showed that the thickness of the PIPGF had little influence on its melting and solidification times. However, the GO concentration had a negative correlation with the melting time and a positive correlation with the solidification time, while the paraffin volume and the volume ratio of paraffin to liquid paraffin had a positive correlation with the melting time and a negative correlation with the solidification time. Thus, to achieve a better temporal resolution, we required PIPGF with higher GO concentration, less paraffin volume, and smaller volume ratio of paraffin to liquid paraffin. Here, considering the effects of the solubility of GO in water, the manipulability of the film, and the convenience of experimental operation, we applied an optimized results of GO (15 mg/ml) and pure paraffin (20 μl/cm^2) to fabricate 300-μm-thick PIPGF for the following experiment.

To demonstrate the practical value of the NIR-controlled programmable wettability pathways, we used the PIPGF for liquid handling in microplate technology. Microplate technology has been accepted as the most reliable platform for biomedical areas. Here, we suggested the PIPGF with programmable wettability for accurately pipetting sample liquids onto microplates (Fig. 5, A and B). The results showed that PIPGF could repel various sample liquids with no residue on the surface and guide them to the desired wells on the microplates along the designed pathways, which greatly simplified the sample pipetting process. Attractively, with designed NIR masks, different samples could be distributed to the same wells, as shown in fig. S5A. Thus, the PIPGF could also be used to achieve gradient concentrations of samples on the microplate wells by controlling the kinds and ratios of the sample droplets (fig. S5B). As the surface wettability of the PIPGF was reversible and programmable, the PIPGF was reusable for sample liquid pipetting in microplates, which reduced the cost of our technology. It is worth mentioning that multiple pathways can be formed with the designed masks; thus, pipetting different samples to different wells can be achieved

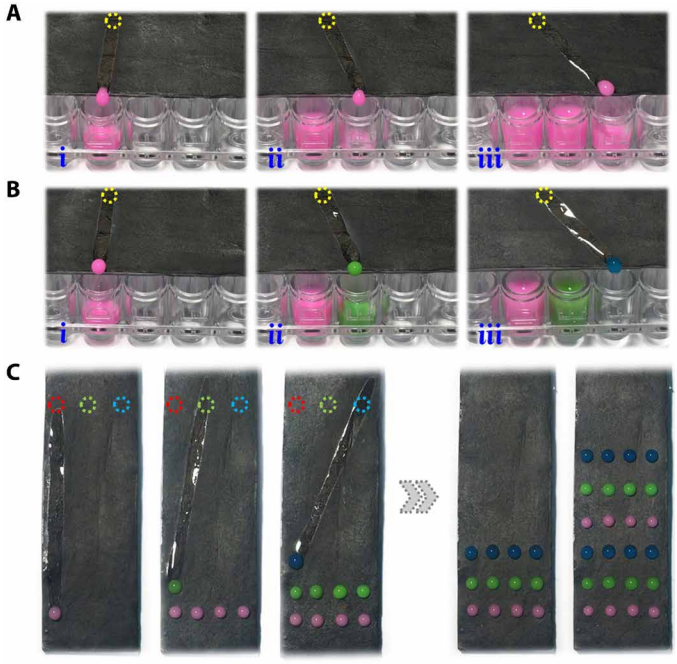

Fig. 5. Progress of applying the PIPGF for pipetting droplets. (**A** and **B**) Pipetting droplets into microplates. The same samples were pipetted into different wells in (A), and the different samples were pipetted into different wells in (B). (**C**) Pipetting droplets to form microarrays on the surfaces of the PIPGF.

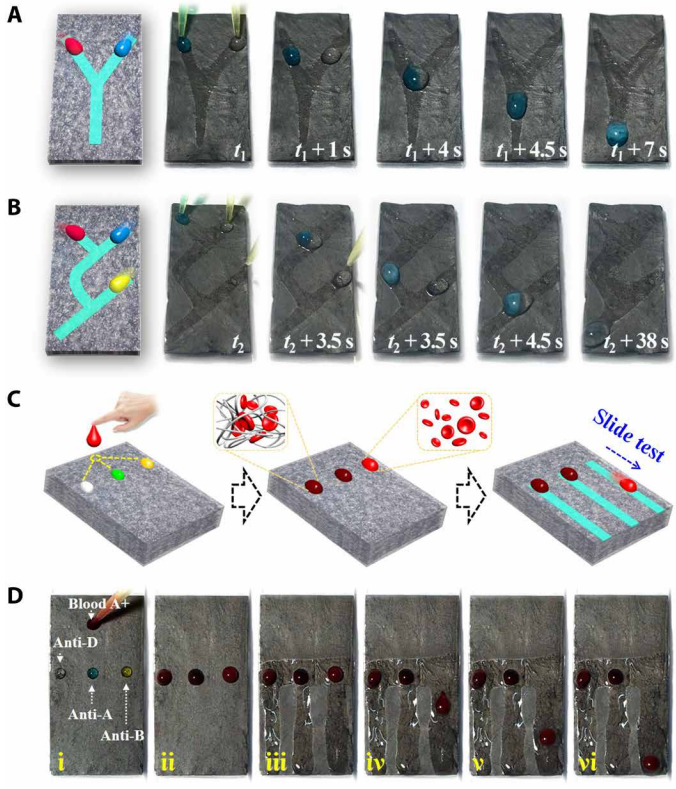

Fig. 6. PIPGF with programmed wettability pathways as microfluidics. (**A** and **B**) Dynamic control of the droplet mobility on the PIPGF surface guided by complicated droplet-guiding pathways with (A) Y-patterned and (B) Y-Y–composite channels. (**C** and **D**) Schematic diagram (C) and progress (D) of using the PIPGF microreactor for grouping the blood sample (A+) by simply monitoring whether the composite blood droplets slid down or not. The antibodies are anti-D, anti-A, and anti-B from left to right in (C) and (D).

at the same time, which saves time compared to manual pipetting. Moreover, by loading samples and changing masks with instruments automatically, it is possible to achieve high-throughput liquid handling for microplates efficiently. Another typical application of NIR-controlled programmable wettability pathways is the fabrication of a droplet microarray on the surface of the PIPGF, as shown in Fig. 5C. With designed pathways, droplets could be accurately distributed to the desired sites without cross-contamination. Thus, various kinds of droplet microarrays could be fabricated on the basis of different droplet samples, which could be beneficial for gene expression analysis, high-throughput screening, and so on.

Besides the simple wettability pathways, the PIPGF with complicated droplet-guiding pathways, such as the Y-patterned and Y-Y–composite channels, could also be programmed, as shown in Fig. 6, fig. S2, and movie S3. These patterned channels could form distinctive microreactors for controllable merging of different types of droplets for chemical reactions. As the results show, a clear blue droplet and a colorless droplet slid down the surface and changed to a composite blue turbid droplet after mixing with each other (Fig. 6A). This was because of the formation of a blue turbid copper metal-organic framework (MOF) in the droplet when the clear blue copper acetate droplet merged with the colorless niacin droplet. However, the generated copper MOF could be degraded by sulfuric acid; thus, the blue turbid droplet changed to a colorless droplet again after meeting the acid droplet (Fig. 6B). This process indicated that the PIPGF could be highly promising for a broad range of applications that were desirable for droplet manipulations and reactions, such as microfluidic systems and laboratory-on-a-chip settings.

To further exploit the value of the PIPGF with complicated droplet-guiding wettability pathways, we used it for human blood grouping (ABO and Rh) in practical diagnosis. Blood grouping is a basic, yet essential, test to be performed before a blood transfusion to avoid the hemolytic reaction. To our knowledge, the presence or absence of antigens (A, B, and D) on the surface of a red blood cell (RBC) is an intrinsic biological property that determines a person's blood group. By monitoring the hemagglutination reaction between the antigens and the antibodies, the person's blood type could be detected. However, the traditional blood grouping methods require observation skills or rely on facilities, as the hemagglutination reaction is not easy to observe. Thus, we presented the use of our PIPGF microreactor for blood grouping by simply monitoring whether the composite blood droplets slid down or not, as schemed in Fig. 6C. During this detection, we guided the blood samples (A+) to mix with the three kinds of antibody (anti-A, anti-B, and anti-D) solutions, respectively, using NIR masks (the first-level pathways), as shown in Fig. 6D and movie S3. We pinned the mixed blood droplets on the surface of the PIPGF for seconds to fully perform the hemagglutination reaction before we subsequently switched on the second-level pathways. The composite blood droplets with no hemagglutination reaction would slide down quickly along the second-level pathways, whereas the droplets would pin on the surface because of precipitation of the agglutinated RBCs if the hemagglutination reaction occurred. We further demonstrated the effectiveness of our PIPGF microreactor in blood grouping by testing two

more types of blood samples (B+ and O+), as shown in fig. S6. We pinned the clotted blood droplets on the surface while others slid down, which was in line with expectations for both of the two blood types. It is worth mentioning that, for this blood grouping application, the volume ratios of the blood droplets to antibody droplets should be limited to the certain range because of its influences on the hemagglutination reaction time and concentration of the agglutinated RBCs (as demonstrated in table S1). Because of the simple operation and the significant results, our PIPGF microreactor could find important roles in clinical blood grouping. It can also be envisioned that our PIPGF will be expanded for a larger number of additional applications by implementing a corresponding droplet-reaction system, such as biological reactions and diagnostic assays.

DISCUSSION

In summary, we have demonstrated a novel PIPGF with photocontrolled programmable wettability. The PIPGF could realize paraffin transition of liquid and solid in response to NIR irradiation because of graphene's photothermal property, resulting in the dynamic and reversible transition between a slippery and a rough surface as remotely tunable wettability. Although other noncontact strategies, such as applying the magnetic responsive fluid to transit interface roughness (*39*) and the ultraviolet-stimulated chemistry and geometry switch of titanium dioxide surface (*40*), also exhibit tunable surface wettability, they are usually limited to poor spatial or temporal resolutions. Generally, the magnetic field could affect the entire surface of the magnetic fluid, and thus, it was difficult to achieve accurate wettability pathways. The titanium dioxide surface fabricated by Hoshian *et al.* (*40*) had the spatial resolution that was as good as 19 μm, while it required minutes of time for switching and even more for recovering. In comparison, by integrating specific NIR masks into the PIPGF system, the paraffin would melt at corresponding patterns on the PIPGF and thus formed special slipping droplet pathways within only tens of seconds. Here, the spatial resolution and temporal resolution of the PIPGF system were about 1 mm and 20 s, respectively. Although other approaches could achieve better spatial or temporal resolutions, the spatiotemporal resolution in our PIPGF system with the combination of spatial resolution and temporal resolution was totally unique and outstanding. Thus, the PIPGF could provide programmable wettability pathways with high spatiotemporal resolution for droplet manipulation by flexibly changing the NIR masks.

On the basis of the intelligent PIPGF, we have also demonstrated that the programmable wettability pathways on the films could not only simplify liquid handling in the microplate and droplet microarrays technology but also provide distinct microfluidic microreactors for different applications, such as practical blood grouping diagnosis. These features indicate that the photocontrollable PIPGF could open new horizons in constructing intelligent droplet microfluidic systems for multidisciplinary community of chemistry, material, energy, health, and so on.

MATERIALS AND METHODS

Materials

The GO solution was bought from Nanjing XFNANO Materials Tech Co. Ltd. HI, calcium chloride ($CaCl_2$), paraffin (melting point, 52° to 54°C), and liquid paraffin were obtained from Aladdin Industrial Corporation. Nicotinic acid and sulfuric acid were purchased from Aladdin Industrial Corporation. Copper acetate monohydrate was bought from Alfa Aesar. Anti-A, anti-B, and anti-D monoclonal blood grouping reagents were from Shanghai Hemo-Pharmaceutical and Biological Co. Ltd. Water with a resistivity of 18.2 megohm·cm^{-1} was acquired from a Millipore Milli-Q system. All other chemical reagents were of the best grade available and used as received.

Fabrication of the porous graphene sponge film

For a typical experiment, GO solution (15 mg/ml) was added to a mold (5 cm in length, 2 cm in width, and 800 μm in thickness), which was prepared with two flat glass slides separated by a rectangle shape spacer and then assembled by the coagulation bath of 5 weight % $CaCl_2$ overnight. The fabricated GO film was subsequently treated with the chemical reduction of 40% HI at room temperature for 24 hours. The film was washed with water to remove the residual iodine and acid and freeze-dried to fabricate porous graphene sponge film.

Fabrication of the PIPGF

The fabricated porous graphene sponge film was immersed in pure melted paraffin in the vacuum oven with the temperature of 80°C under vacuum for 2 hours to totally replace the pores in the film with paraffin. The excess residual paraffin on the surface was span and removed to construct the PIPGF with pure paraffin (20 μl/cm^2).

Patterned flow pathways of the PIPGF

Masks were used between the fabricated PIPGF (around 4 cm in length and 1.5 cm in width) and the laser to form the patterned flow pathways on the surface of the film. The laser was uniform for the 3 cm × 3 cm irradiation area with a power intensity of 1.6 W/cm^2. Part of the laser could go through the masks to the film surface, which made the irradiated paraffin melt at the corresponding pattern. By changing different masks, different flow pathways of the PIPGF could be fabricated.

Blood grouping using the PIPGF

Three blood samples of known types were acquired and stored in Vacutainer test tubes containing lithium-heparin anticoagulant from Zhongda Hospital in Nanjing, China. This protocol was approved by the institution's Ethics Committee according to the provisions of the Declaration of Helsinki regarding investigation in humans. Three kinds of antibody solutions were also added with lithium-heparin anticoagulant in the experiments. The amount of the mixed blood samples was kept the same for testing. The porous graphene film was infused with the mixture of solidifiable paraffin and the liquid paraffin at the volume ratio of 1:1 in this section. The blood plasma was removed from the blood samples.

Characterization

The SEM images were obtained using a SEM (Hitachi S-3000N). Colored photos and videos were taken on a digital camera (Canon 5D Mark II). Water contact angles were obtained by a JC2000D2 contact angle measuring system at ambient temperature. Sliding angles were measured on a customized tilting stage with a droplet volume of 6 μl. Static contact angles were recorded with a droplet volume of 2 μl. The static contact angles were measured at a neutral tilting angle (0°). The numbers of replicates for the three different

contact angle measuring groups were all four. The NIR irradiation (808 nm; Xi Long Tech Co. Ltd.) was used with the power intensity of 1.6 W/cm^2. The temperature of the PIPGF was recorded by the uncooled handheld infrared camera (FLIR Systems AB).

SUPPLEMENTARY MATERIALS

Supplementary material for this article is available at http://advances.sciencemag.org/cgi/content/full/4/9/eaat7392/DC1

Fig. S1. Optical images of the PIPGF.
Fig. S2. Recorded temperature of the PIPGF with different pathways.
Fig. S3. Temperature change of the PIPGF during melting and solidification.
Fig. S4. Melting and solidification times of the PIPGF.
Fig. S5. Distributing different sample droplets.
Fig. S6. PIPGF microreactor for grouping the blood samples B+ and O+.
Table S1. Clotting times and sliding properties of the mixed blood droplets with different volume ratios of blood (A+) to antibody (anti-A).
Movie S1. Droplet mobility on a tilted PIPGF surface.
Movie S2. Programmed wettability pathways.
Movie S3. Manipulating droplet reactions and blood grouping.

REFERENCES AND NOTES

1. X. Tian, T. Verho, R. H. A. Ras, Moving superhydrophobic surfaces toward real-world applications. *Science* **352**, 142–143 (2016).
2. H. Kim, S. Yang, S. R. Rao, S. Narayanan, E. A. Kapustin, H. Furukawa, A. S. Umans, O. M. Yaghi, E. N. Wang, Water harvesting from air with metal-organic frameworks powered by natural sunlight. *Science* **356**, 430–434 (2017).
3. B. Su, Y. Tian, L. Jiang, Bioinspired interfaces with superwettability: From materials to chemistry. *J. Am. Chem. Soc.* **138**, 1727–1748 (2016).
4. A. Abbaspourrad, N. J. Carroll, S.-H. Kim, D. A. Weitz, Surface functionalized hydrophobic porous particles toward water treatment application. *Adv. Mater.* **25**, 3215–3221 (2013).
5. Y. J. Zhao, H. Gu, Z. Xie, H. C. Shum, B. Wang, Z. Gu, Bioinspired multifunctional Janus particles for droplet manipulation. *J. Am. Chem. Soc.* **135**, 54–57 (2013).
6. S. Huang, D. Wang, A simple nanocelloluse coating for self-cleaning upon water action: Molecular design of stable surface hydrophilicity. *Angew. Chem. Int. Ed.* **56**, 9053–9057 (2017).
7. M. He, Y. Ding, J. Chen, Y. Song, Spontaneous uphill movement and self-removal of condensates on hierarchical tower-like arrays. *ACS Nano* **10**, 9456–9462 (2016).
8. T. Mouterde, G. Lehoucq, S. Xavier, A. Checco, C. T. Black, A. Rahman, T. Midavaine, C. Clanet, D. Quéré, Antifogging abilities of model nanotextures. *Nat. Mater.* **16**, 658–663 (2017).
9. Y. Zhang, Y. Li, P. Ming, Q. Zhang, T. Liu, L. Jiang, Q. Cheng, Ultrastrong bioinspired graphene-based fibers via synergistic toughening. *Adv. Mater.* **28**, 2834–2839 (2016).
10. L. Shang, Y. Wang, Y. Yu, J. Wang, Z. Zhao, H. Xua, Y. Zhao, Bio-inspired stimuli-responsive graphene oxide fibers from microfluidics. *J. Mater. Chem. A* **5**, 15026–15030 (2017).
11. M. Liu, S. Wang, L. Jiang, Nature-inspired superwettability systems. *Nat. Rev. Mater.* **2**, 17036 (2017).
12. H. Chen, P. Zhang, L. Zhang, H. Liu, Y. Jiang, D. Zhang, Z. Han, L. Jiang, Continuous directional water transport on the peristome surface of *Nepenthes alata*. *Nature* **532**, 85–89 (2016).
13. Y. Zhao, Y. Wu, L. Wang, M. Zhang, X. Chen, M. Liu, J. Fan, J. Liu, F Zhou, Z. Wang, Bio-inspired reversible underwater adhesive. *Nat. Commun.* **8**, 2218 (2017).
14. K.-C. Park, P. Kim, A. Grinthal, N. He, D. Fox, J. C. Weaver, J. Aizenberg, Condensation on slippery asymmetric bumps. *Nature* **531**, 78–82 (2016).
15. L. Shang, F. Fu, Y. Cheng, Y. Yu, J. Wang, Z. Gu, Y. Zhao, Bioinspired multifunctional spindle-knotted microfibers from microfluidics. *Small* **13**, 1600286 (2017).
16. T.-S. Wong, S. H. Kang, S. K. Y. Tang, E. J. Smythe, B. D. Hatton, A. Grinthal, J. Aizenberg, Bioinspired self-repairing slippery surfaces with pressure-stable omniphobicity. *Nature* **477**, 443–447 (2011).
17. K. Manabe, T. Matsubayashi, M. Tenjimbayashi, T. Moriya, Y. Tsuge, K.-H. Kyung, S. Shiratori, Controllable broadband optical transparency and wettability switching of temperature-activated solid/liquid-infused nanofibrous membranes. *ACS Nano* **10**, 9387–9396 (2016).
18. J. D. Smith, R. Dhiman, S. Anand, E. Reza-Garduno, R. E. Cohen, G. H. McKinleya, K. K. Varanasi, Droplet mobility on lubricant-impregnated surfaces. *Soft Matter* **9**, 1772–1780 (2013).
19. S. Amini, S. Kolle, L. Petrone, O. Ahanotu, S. Sunny, C. N. Sutanto, S. Hoon, L. Cohen, J. C. Weaver, J. Aizenberg, N. Vogel, A. Miserez, Preventing mussel adhesion using lubricant-infused materials. *Science* **357**, 668–673 (2017).
20. D. Daniel, J. V. I. Timonen, R. Li, S. J. Velling, J. Aizenberg, Oleoplaning droplets on lubricated surfaces. *Nat. Phys.* **13**, 1020–1025 (2017).
21. X. Yao, Y. Hu, A. Grinthal, T.-S. Wong, L. Mahadevan, J. Aizenberg, Adaptive fluid-infused porous films with tunable transparency and wettability. *Nat. Mater.* **12**, 529–534 (2013).
22. C. Liu, H. Ding, Z. Wu, B. Gao, F. Fu, L. Shang, Z. Gu, Y. Zhao, Tunable structural color surfaces with visually self-reporting wettability. *Adv. Funct. Mater.* **26**, 7937–7942 (2016).
23. J. Kamei, H. Yabu, On-demand liquid transportation using bioinspired omniphobic lubricated surfaces based on self-organized honeycomb and pincushion films. *Adv. Funct. Mater.* **25**, 4195–4201 (2015).
24. J. Wang, L. Sun, M. Zou, W. Gao, C. Liu, L. Shang, Z. Gu, Y. Zhao, Bioinspired shape-memory graphene film with tunable wettability. *Sci. Adv.* **3**, e1700004 (2017).
25. Y. Zhang, S. Gong, Q. Zhang, P. Ming, S. Wan, J. Peng, L. Jiang, Q. Cheng, Graphene-based artificial nacre nanocomposites. *Chem. Soc. Rev.* **45**, 2378–2395 (2016).
26. T. Gao, X. Song, H. Du, Y. Nie, Y. Chen, Q. Ji, J. Sun, Y. Yang, Y. Zhang, Z. Liu, Temperature-triggered chemical switching growth of in-plane and vertically stacked graphene-boron nitride heterostructures. *Nat. Commun.* **6**, 6835 (2015).
27. X. Yu, H. Cheng, M. Zhang, Y. Zhao, L. Qu, G. Shi, Graphene-based smart materials. *Nat. Rev. Mater.* **2**, 17046 (2017).
28. H. Cheng, Y. Huang, G. Shi, L. Jiang, L. Qu, Graphene-based functional architectures: Sheets regulation and macrostructure construction toward actuators and power generators. *Acc. Chem. Res.* **50**, 1663–1671 (2017).
29. J. Wang, L. Shang, Y. Cheng, H. Ding, Y. Zhao, Z. Gu, Microfluidic generation of porous particles encapsulating spongy graphene for oil absorption. *Small* **11**, 3890–3895 (2015).
30. X. Gao, J. Zhou, R. Du, Z. Xie, S. Deng, R. Liu, Z. Liu, J. Zhang, Robust superhydrophobic foam: A graphdiyne-based hierarchical architecture for oil/water separation. *Adv. Mater.* **26**, 168–173 (2016).
31. B. Yao, J. Chen, L. Huang, Q. Zhou, G. Shi, Base-induced liquid crystals of graphene oxide for preparing elastic graphene foams with long-range ordered microstructures. *Adv. Mater.* **28**, 1623–1629 (2016).
32. Z. Zhao, H. Wang, L. Shang, Y. Yu, F. Fu, Y. Zhao, Z. Gu, Bioinspired heterogeneous structural color stripes from capillaries. *Adv. Mater.* **29**, 1704569 (2017).
33. J. N. Wilking, V. Zaburdaev, M. De Volder, R. Losick, M. P. Brenner, D. A. Weitz, Liquid transport facilitated by channels in *Bacillus subtilis* biofilms. *Proc. Natl. Acad. Sci. U.S.A.* **110**, 848–852 (2013).
34. J. Li, X. Zhou, J. Li, L. Che, J. Yao, G. McHale, M. K. Chaudhury, Z. Wang, Topological liquid diode. *Sci. Adv.* **3**, eaao3530 (2017).
35. K.-H. Chu, R. Xiao, E. N. Wang, Uni-directional liquid spreading on asymmetric nanostructured surfaces. *Nat. Mater.* **9**, 413–417 (2010).
36. L. Shang, Y. Cheng, Y. Zhao, Emerging droplet microfluidics. *Chem. Rev.* **117**, 7964–8040 (2017).
37. Y. Li, D. Quéré, C. Lv, Q. Zheng, Monostable superrepellent materials. *Proc. Natl. Acad. Sci. U.S.A.* **114**, 3387–3392 (2017).
38. D. Chen, G. H. McKinley, R. E. Cohen, Spontaneous wettability patterning via creasing instability. *Proc. Natl. Acad. Sci. U.S.A.* **113**, 8087–8092 (2016).
39. D. Tian, N. Zhang, X. Zheng, G. Hou, Y. Tian, Y. Du, L. Jiang, S. X. Dou, Fast responsive and controllable liquid transport on a magnetic fluid/nanoarray composite interface. *ACS Nano* **10**, 6220–6226 (2016).
40. S. Hoshian, V. Jokinen, K. Hjort, R. H. A. Ras, S. Franssila, Amplified and localized photoswitching of TiO_2 by micro- and nanostructuring. *ACS Appl. Mater. Interfaces* **7**, 15593–15599 (2015).

Acknowledgments

Funding: This work was supported by the National Natural Science Foundation of China (grant nos. 51725602, 51522302, and 21473029) and the NSAF Foundation of China (grant no. U1530260). **Author contributions:** Y.Z. and Y.C. conceived the idea and designed the experiment. J.W. and W.G. carried out the experiments. J.W. and Y.Z. analyzed the data and wrote the paper. H.Z., M.Z., and Y.C. contributed to scientific discussion of the article. J.W. and W.G. contributed equally to this work. **Competing interests:** The authors declare that they have no competing interests. **Data and materials availability:** All data needed to evaluate the conclusions in the paper are present in the paper and/or the Supplementary Materials. Additional data related to this paper may be requested from the authors.

Submitted 29 March 2018
Accepted 7 August 2018
Published 14 September 2018
10.1126/sciadv.aat7392

Citation: J. Wang, W. Gao, H. Zhang, M. Zou, Y. Chen, Y. Zhao, Programmable wettability on photocontrolled graphene film. *Sci. Adv.* **4**, eaat7392 (2018).

Programmable wettability on photocontrolled graphene film

Jie Wang, Wei Gao, Han Zhang, Minhan Zou, Yongping Chen and Yuanjin Zhao

Sci Adv **4** (9), eaat7392.
DOI: 10.1126/sciadv.aat7392